



ELSEVIER

Available online at www.sciencedirect.com
jmr&t
 Journal of Materials Research and Technology
journal homepage: www.elsevier.com/locate/jmrt**Original Article**

Effects of sand and gating architecture on the performance of foot valve lever casting components used in pump industries

I. Rajkumar ^a, N. Rajini ^{a,*}, Suchart Siengchin ^{b,**},
 Sikiru Oluwarotimi Ismail ^c, Faruq Mohammad ^d, Hamad A. Al-Lohedan ^d,
 Ahmed M. Tawfeek ^d, Zuheir A. Issa ^d

^a International Research Center, Kalasalingam Academy of Research and Education, Krishnankoil, 626126, India

^b Department of Materials and Production Engineering, The Sirindhorn International Thai-German Graduate School of Engineering (TGGs), King Mongkut's University of Technology North Bangkok, 1518 Wongsawang Road, Bangsue, Bangkok, 10800, Thailand

^c Department of Engineering, School of Physics, Engineering and Computer Science, University of Hertfordshire, Hatfield, AL10 9AB, Hertfordshire, England, United Kingdom

^d Department of Chemistry, College of Science, King Saud University, Riyadh, 11451, Saudi Arabia

ARTICLE INFO**Article history:**

Received 21 June 2021

Accepted 18 August 2021

Available online 4 September 2021

Keywords:

Sand types

Gating designs

Surface roughness

Porosity

Simulation

Experiment

ABSTRACT

This work addresses manufacture, testing and simulation of foot valve lever (FVL) for monoblock pump industry, using a cost-effective casting design process. The impact of different types of sands, such as air-set, dry and sodium silicate as well as gating designs, namely H-, U- and O-type, were studied with respect to surface roughness and porosity. The mold pattern was produced using additive manufacturing (AM) technology. Both experimental and numerical investigations were performed on the temperature distribution of molten metal at random locations for the different gating configurations or designs, considering mold filling and solidification. It was evident from the experimental investigation that contribution of air-set sand and O-type gating architecture showed limited consistency effects. Importantly, gating architecture was the most influential parameter to determine all specified quality outcomes, independent of sand mold. An order of O < H < U-type was obtained from the gating designs for minimal surface roughness and percentage of porosity. Furthermore, the microstructure analysis depicted only an irregular defect with minimum quantity at both surface and cross-section of O-type at two different locations. Optimum pouring temperatures of 740, 750 and 790 °C were obtained for mold filling of all 24 components of H-, O- and U-type of gating designs, respectively. The varying solidification temperature was observed from real time thermocouple reading, which was in close agreement with the numerical simulation. Evidently, O-type of gating design

* Corresponding author.

** Corresponding author.

E-mail addresses: rajiniklu@gmail.com (N. Rajini), suchart.s.pe@tggbs-bangkok.org (S. Siengchin).

<https://doi.org/10.1016/j.jmrt.2021.08.125>

2238-7854/© 2021 The Author(s). Published by Elsevier B.V. This is an open access article under the CC BY-NC-ND license (<http://creativecommons.org/licenses/by-nc-nd/4.0/>).

exhibited best performance for large-scale development of the FVL in terms of surface roughness, porosity and cooling effects.

© 2021 The Author(s). Published by Elsevier B.V. This is an open access article under the CC BY-NC-ND license (<http://creativecommons.org/licenses/by-nc-nd/4.0/>).

1. Introduction

While technical progress is imminent in manufacturing sectors, certain conventional approaches limit functions or capabilities of small-scale factories to attain a greater level. Accordingly, design of novel materials with enhanced mechanical, wear, friction properties and their microstructure characterization obtained through various casting processes seek more attention among casting analysts [1–3]. For instance, application of a sand casting process essentially leads to production of casting components in many engineering industries. In general, sand casting process is affected by different parameters, such as casting orientation, feeder configuration, molten metal temperature, sand properties (grain size and bonding material), riser geometry, riser position, chill properties and chill location. All these parameters can have effects on performance of the final products with different spectrum of limits. It is therefore necessary to choose relevant criteria that have better effects on the quality characteristics based on customer's requirements. In this regard, numerous works have been reported to resolve various concerns of manufacturers on their final products, taking into account the impact of sand-casting parameters [4,5].

To understand the result of casting products, various kinds of sands have been investigated for varied characteristics of the manufactured components [6]. For instance, in a recent study [7], travertine powder, travertine sludge and fine sand were used to create fake stone in the mold sand. Their effects on input factors, including curing temperature, epoxy resin type, percentage of solid components, and proportion of epoxy resin per solid components were examined. The results indicated that each variable has a distinct influence on the compressive and flexural strengths of the stones of different groups. In other study [8], poly-ethylene terephthalate (PET) polymers were utilized as a partial replacement for sand in concrete. The effects of this material on the physical and mechanical characteristics of concrete were investigated. The results indicated a decrease in unit weight. It was observed that sand substitution damaged the mechanical characteristics of the concrete at different rates. Also, it was evident that plastic waste can be disposed of in specified ratios, and therefore it can be used efficiently in industrial sectors. Despite of the fact that numerous works have been studied on the sand-casting process, there is still a possibility of getting excellent outcomes with different variables linked to the sand-casting process. This has challenged many researchers to utilize cutting-edge technology.

Besides, growing popularity in small-scale casting industries includes the use of numerous user-friendly simulation approaches to model and solve some complex and intricate cast

components. Furthermore, output characteristics such as mold filling and solidification, hot spot region and other susceptible defects can also be simulated to a greater precision, using these tools. With in-built special features, there are many casting simulations available in the market to bridge difference between simulation and real time casting processes. Most importantly, these tools are effectively used to replace expensive "trial and error" shop floor sessions to determine optimum parameters for production of quality castings, mold filling and solidification simulations. Therefore, it leads to reduction in rejects, saving time and cost [9]. In this direction, the advancement computer-aided design (CAD) models and simulation on casting solidification can enable foundry engineers and industrial metallurgists to investigate various factors, using simulation tools. Accordingly, influence of hot spot region has been reported, using time-temperature contours and provided information about merits and demerits, based on the simulation results [10,11].

In addition, pouring temperature was identified as most important factor affecting quality of Al–Si–Cu foam casting [12]. The effect of thermocouples on temperature measurements was analyzed numerically and experimentally, considering solidification of thin wall castings, and the measures required to ensure correct acquisition of cooling curves were addressed [13]. The results showed the accuracy of casting, using Auto CAST software by running the whole method, optimization followed the simulation. Based on the study and after comparison, it was observed that experimental test and simulation results were in agreement consistently [14]. Moreover, the performance of these tools in the real time casting products also showed encouraging results.

Also, pulp valve part, made of cast iron, was studied in conjunction with both Solid-Cast simulation software and experimentation. The study showed a significant advantage of development of effective gating and feeding devices, which could improve casting yield and performance as well as reduce internal defects. Substantial quality components, time and expense needed for shop floor testing can be saved by casting simulation [15]. In another study, movement of molten metals, such as mold filling, solidification and cooling, as well as prediction of position of internal defects, were analyzed, using simulation results [16,17]. The sand casting of a crusher plate was carried out with Pro Cast programme, which is popular in current casting industry. Intelligent use of this simulation software makes it possible to increase amount of scrap for optimum design considerations. Several studies [18] have enabled identification of errors with good confidence and good performance elements. The modules were redesigned using technical knowledge, feed laws, historical background and gating rules, and then introduced using the Auto

CAST-X flow plus simulation programme [19]. The best design was ultimately projected and compared with experimental findings of casting process [20,21]. In non-pressurized gating systems, there is a discrepancy of melt flow from centre line of mold or irregular filling of the gate [22,23]. Experimental investigation into significance of using cost-effective approach of fused deposition modelling has been carried out. The results showed substantial improvements on mechanical properties and reduced porosity [24]. However, the applicability of these tools in the real time casting products were observed to be scanty.

Importantly, monoblock pump industry is one of the main companies that are selling components for water storage to various sectors, such as domestic, industrial, chemical and manufacturing. There is a component called foot valve lever (FVL) in the configuration of all pump types, which stops the reverse flow of water back to the sump. In general, FVL was developed by small scale casting factories, using gun metal to resist corrosion under water conditions. However, attention must be paid to mass production by monitoring different essential criteria in order to achieve a quality part. Hence, in a

bid to enhance quality and performance of FVL, the current work is conducted. FVL was fabricated mainly for mass production in compliance with time limit and mold dimension, as prescribed by its manufacturer. For all customer specifications, parameters such as casting orientations, types of sands and gating designs were analyzed, using both experimentation and numerical simulation comparatively. In addition, additive manufacturing (AM) method was used to produce intricate patterns with a 24-cavity complex runner for a stepped bar of different aspect ratios (l/d), using a sand-casting process. This analysis was carried out with intention of minimizing errors, reducing refuse rate, shop floor trials and lead time for production of FVL. Also, a cost effective complex multi-cavity runner system was used.

2. Materials and experimental methods

FVL casting component, its complexity and mass production were considered for both numerical and experimental studies. Previously, gunmetal was used as raw material for

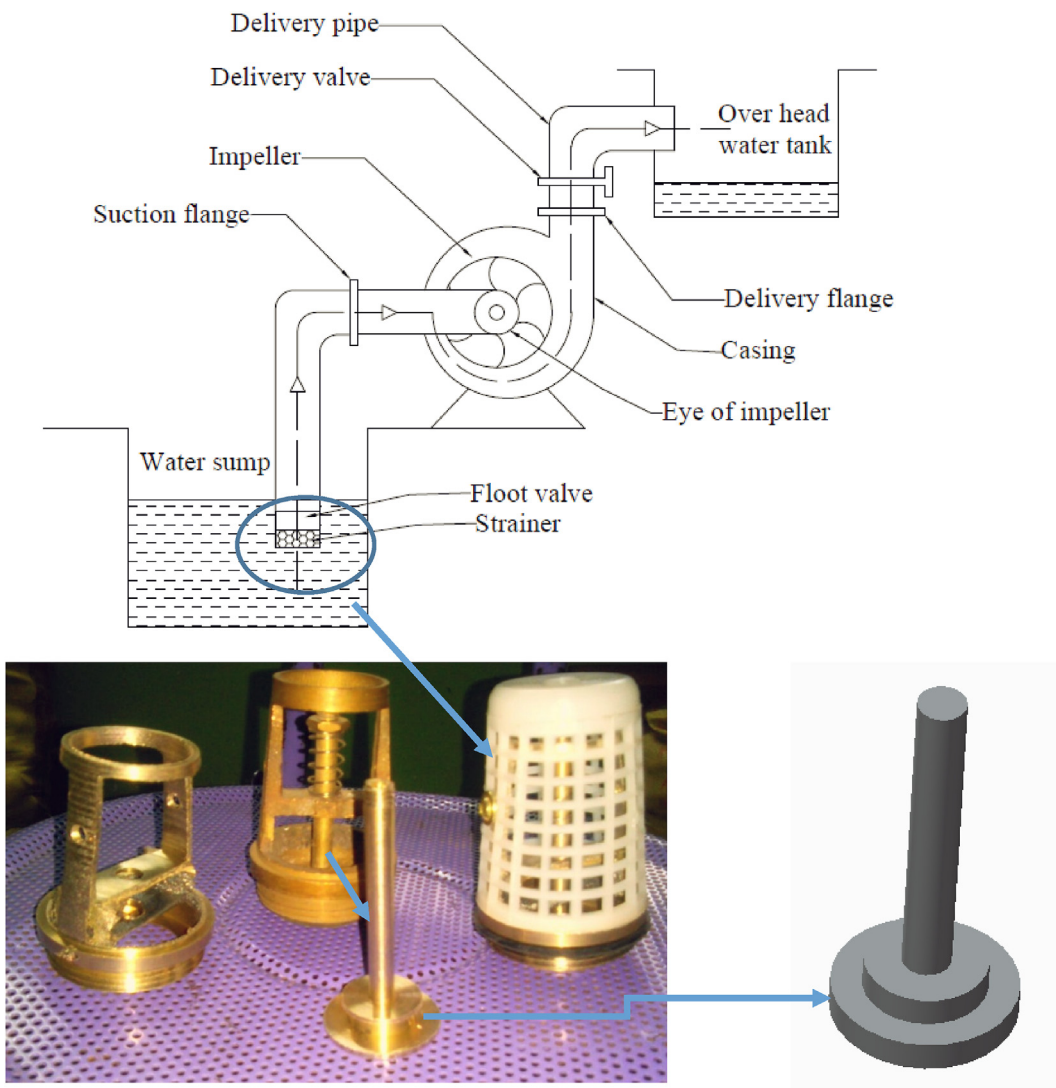


Fig. 1 – Foot valve assembly in a Monoblock pump and FVL configuration.

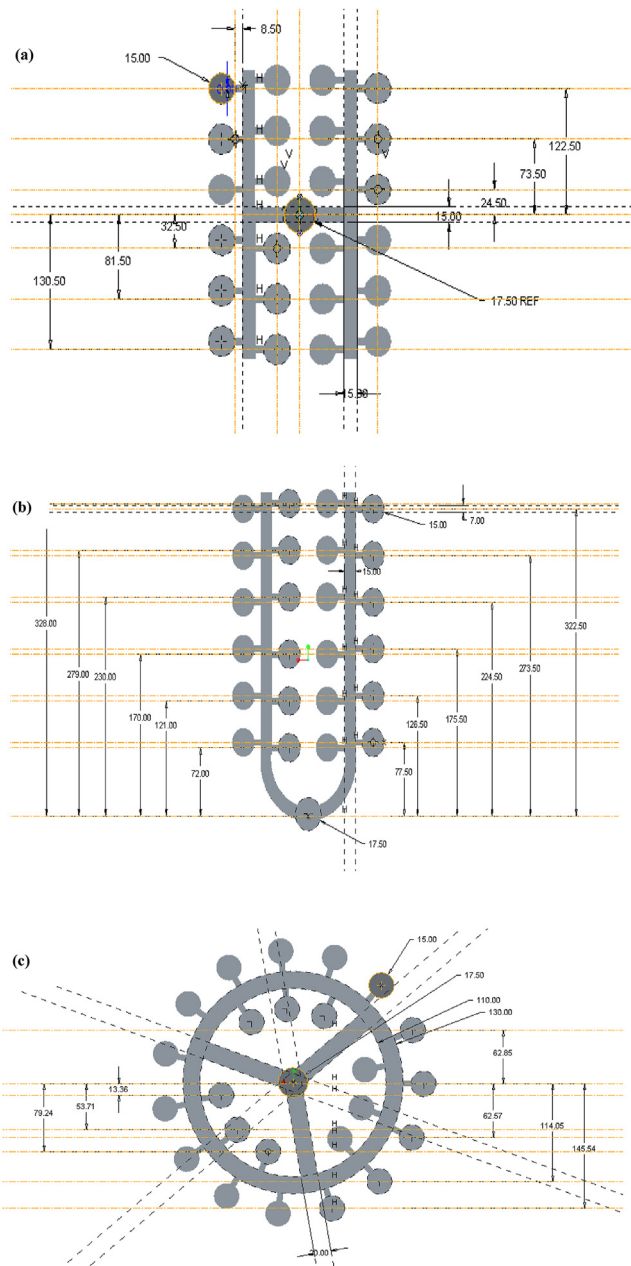


Fig. 2 – Geometry dimensions of (a) H-, (b) O- and (c) U-type of molds.

manufacturing FVL, but its cost is too high, therefore the experimental target was to use LM25 (Al–Si7Mg) metal. The experimental study centred on influencing parameters, such as various gating geometries and types of sands as well as their effects on surface roughness and porosity, using aforementioned metal alloy. Fig. 1 indicates the position of the foot valve assembly in a mono block pump and FVL design extraction.

Based on the specified measurements, CAD model of FVL was built with dimensions; diameters of 30, 20 and 8 mm and pulling lever length of 55 mm, using SolidWorks. In order to minimize its weight, steel mold was substituted with poly-(lactic acid) thermoplastic polymer. The fusion disposition modelling (FDM) was used to manufacture the different

patterns, using PLA, which has considerable strength to create a cavity in the mold. In addition, the smooth interface was required to improve the materials and consequently increase quality of metal flow from the pattern. PLA filament, with a diameter of 1.75 mm, was used for processing, which was capable of generating intricate parts in a preferable manner.

There were three phases of FDM process: pre-processing, production and post-processing. The model was translated to a STL file to read the data for initiation of the printing process. Also, at this stage, operations such as slicing feature, tool-path generation, component orientation and support system were conducted. Optimum processing parameters that are capable of yielding better mechanical properties were used to create appropriate patterns [25].

The creation stage is the internal processing period where material is added layer by layer until production of the part is finished per a unit. The burrs were separated from the template during the last stage. Afterwards, polishing and cleaning of the printed pieces took place. The top views (plans) of geometrical dimensions of H-, U- and O-type of gating designs are shown in Fig. 2.

There is a possibility of catastrophic failure at the lower part of the FVL made up of low strength PLA polymer, due to buckling force during sand impact on the mold. Mold breakage was detected at the moment of component development. The pattern was then split into two parts, one runner, gate and FVL, and another segment as a spur poring basin. Afterwards, in the flat rectangular board, the split pattern was pasted, which was a reasonably simple way to produce cavity in the mold without any pattern failure. During the fabrication, three samples were made for each of the three kinds of gating designs per type of sand to confirm repeatability of FVL.

3. Simulation tools and procedure

C3P Cast-Designer simulation tool was used in this analysis to carry out FVL part simulation. This software package uses finite element technique to mesh three dimensional (3D) real-time casting products in the most economical way. The program simulated the flow of molten metal, using famous Navier–Stokes' equation and enthalpy principle to analyze the solidification process. Moreover, the result provided a visual information related to the movement of dynamic heat source and their influences at various pouring temperatures. During the simulation process, all relevant parameters and boundary conditions were selected, similar to the experimental condition for the fabrication of FVL component. STL CAD model files were inserted for programming, as a first step. Then, the model was meshed to perform the simulation. Finally, the outcomes were plotted and evaluated to determine whether the simulation is to be re-run or redesigned.

4. Preparation of different molding sands

Three forms of sands were prepared. They were air-set, sodium silicate and dry sands. During preparation of sands, parameters such as grain fineness quantity of 55 GFN, ramming quantity of two times, degassing quantity of 1% of total

Table 1 – Thermocouple points of locations and justifications.

TC	Location	Justification
1	The TC1 point was located on the right side top corner outer side, close to the mold box area.	To calculate volume of cooling that happened at metal mold interface of side wall.
2	Placed 95 × 106 mm away from TC3 and put in mold side wall thickness area (interface between sand and mold box)	To determine how much heat-absorbing sand mold was in the surrounding cavity region.
3	This TC point was positioned on the right side runner inner side as well as the top centre metal mold interface field U-type, which was very close to the sprue and half circle runner. The O-type was observed outside the outer diameter region.	This argument justified the amount of temperature in the component centre in both H- and O-type. Half circle main runner temperature fluctuations were observed by the U-type – TC point.
4	This TC point was positioned on the left runner, next to the sprue position and the top middle metal mold interface. A U-shaped TC point was located in the middle of the left runner. O-type TC point positioned within the diameter region, close to the sprue spot.	To determine the amount of temperature loss in the outer side of the left runner of H- and U-type of gating designs. Calculate the amount of heat consumed by the main runner.
5	For both H- and U-type of designs, it (TC5) was located on the left side end outside position and in the top centre metal mold interface region. The inner circle was divided into three sections, each with three components, the middle of it was a TC point in O-type.	In H- and U-type of designs, to absorb the amount of cooling effects in the middle of the component. Temperature was absorbed from surrounding O-type components.

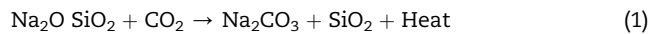
metal by weight, holding period of 2 min and alloy form A356 were held constant, as described in previous works [26,27]. Part descriptions and method of preparing various forms of sands are subsequently and clearly elucidated.

4.1. Air-set sand

This form of sand was formulated with a chemical mixture of silica sand and three-part alkyd resin. In part A for the blending, 2% alkyd resin alone was taken. An activator of 3–8% of component of an alkyd resin was used to prepare part B. Catalyst was eventually prepared in part C with 15–20% of part A alkyd resin. Parts A and B were initially pre-mixed during mixing phase, before being added to the silica sand and permitted to stay for 2–4 min. Then, the mixture was applied to Part C and reworked again for 1 min. Both of these operations have to be conducted by incorporating catalyst between 12 and 15 min to prevent accelerated chemical healing. Depending on complexity and composition of the mold and conditions, the mold has a span of 40–45 min.

4.2. Sodium silicate sand

Silica sand was combined with 1.5–6.0% of sodium silicate solution, also known as silica gel or water glass. It acted as a binder. The silica sand and the binder were kept for 10 min and the sand mixture was used to create the molds. The molds were then reinforced with carbon dioxide (CO_2) gas (Eq. (1)), streaming through them for a few seconds at a pressure of 1.5–2.0 kg/cm². Initially, the holes covering the cavity were generated for this method and the CO_2 gas was supplied through these holes. The effect of heat altered properties of the sand to cause escape of gas during pouring of molten metal.



4.3. Dry sand

Traditional green sand casting method uses 75–85% of silica sand molds mixed with 5–12% of bentonite, 2–4% of water and 0–3% of other additives to boost their strength, permeability and collapsibility. All the materials were transferred to muller and mulled for 15 min. The molds were primed, using green sand and allowed to dry for 48–72 h, before pouring. Experiments were conducted to manufacture 24 FVL casting parts from all the aforementioned sand types for the various gating designs and pouring temperatures.

5. Results and discussion

5.1. Simulation analysis of different gating systems

3D model of FVL parts with different gating designs were translated to STL files and then inserted into Cast-Designer simulation software. Output parameters, such as mold filling, cooling and solidification were analyzed at various pouring temperatures to predict consistency of the casting

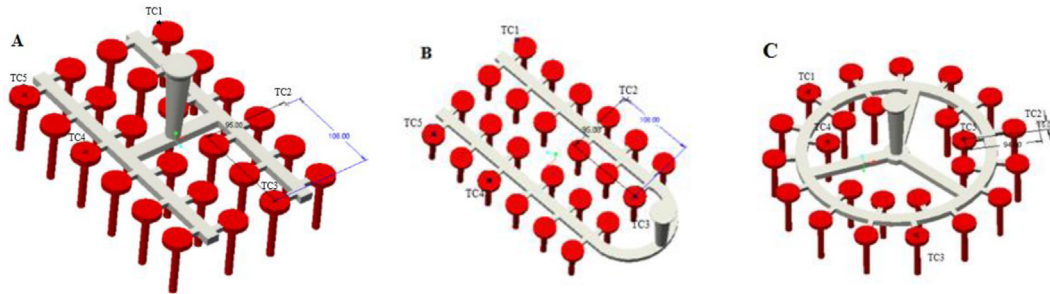


Fig. 3 – Location of thermocouple points in 3D model of FVL components for (A) H-, (B) U- and (C) O-type of gating designs.

components. The configuration of the mold and space restriction were maintained according to the industry specification for development of FVL parts. Temperature scale ranged from 710 to 790 °C., all the three gating architectures.

In addition, it was observed from the result of this study that all cavities of H-type of gating configuration were filled at a lower pouring temperature of 740 °C. On the other side, at this same pouring temperature, 50 and 80% of cavity filling was observed with both U- and O-style gating design. Finally, the maximum mold filling of O- and U-type of gating designs were observed at pouring temperatures of 750 and 790 °C, respectively. From the visual observation, it was observed that the layout of the runner played a crucial role to decide on cavity filling pattern of mold. Although, the other variables such as gating distance and sprue height were maintained as constant measurements in all the three situations.

In an attempt to consider the cooling effect and solidification of molten metal, five thermocouples were placed in each type of the gating designs at separate locations of the mold based on proper rationales, as presented in Table 1. Fig. 3 shows positions of the thermocouples for each form of gating design. Thermocouples (TC) were held at the same locations in the 3D model to document temperature data for each 5 s throughout simulation phase.

Furthermore, a number of simulations were done by changing pouring temperature for the different gating designs to ensure that the filling sequence took place without misruns, cold-shuts or unfilled sections in the cavities. From H-type gating design, the process of mold filling was analyzed for three separate time intervals of 1.9, 3.3 and 5.3 s at optimum pouring temperature of 740 °C, as shown in Fig. 4. During initial time, the whole runner and gate length were flooded with molten metal, and the first cavity closest to the cross runner began to fill up. Following this, the metal loading in the cavity improved, while the duration increased. In the course of complete filling, both left and right end components were finally identified to achieve solidification. Similarly, the mold filling in U-type was analyzed at a pouring temperature of 790 °C over an approximately equivalent time period, as shown in the H-type. However, only the runner and a few gate lengths were filled with molten metal even at this higher temperature. At 5.3 s, nearly all the cavities were saturated with various cooling temperatures.

Two neighbouring sets of cavities, situated at the free end (opposite side to sprue) were observed to be cooled, which was

predicted to occur due to the location of those at a higher distance from the discharge stage. However, the findings indicated that the cooling rate was considerably lower in the case of U-type, which can be attributed to higher input temperature than that of H-type. In addition, the location of the cavity enclosed by the molding sand was also a crucial parameter to decide the rate of cooling in the sand molding phase. Consequently, cavity at the metal mold interface, where the thickness of the mold was high, implied a higher cooling rate than the lower thickness of the mold.

From O-type gating design, input temperature was selected as 750 °C, which was responsible for the complete mold filling. It generated a better percentage of mold filling at time interval of 3.3 s than that of other types. At same time, the rate of cooling occurred rapidly in most of the cavities of O-type. Since more components were present in the outer circumference, they were connected directly with thick wall of the molding sand. In comparison, the inner wall thickness (distance between inner circle components and centre of sprue) of the mold was also considerably large when compared with the other two cases. As a result, almost 90% of the components cooled at the time of mold filling, which reduced the chances of air trapping, porosity and shrinkage. However, this design method can increase the probability of having a cold shut defect at point of fluid junction.

Side view of the needles, as a part of FVL component and its solidification rate, were extracted with respect to different locations. In the case of H-type, an accurate solidification symmetry was obtained with respect to the cross-runner. In other side, the fin at the far end of the sprue displayed a greater solidification than that of the closest discharge point at the U-type runner. Whereas, in the case of O-type of construction, the needles of the outer components solidified quicker than those of inner components. However, all fins were solidified at time of mold filling. Regardless of the type of gating system, high modulus component was eventually solidified uniformly in case of O-type of design.

5.2. Temperature–time history

5.2.1. Simulation

Temperature plots of the different gating designs obtained at 500 s are shown in Fig. 5(a)–(c). All data were collected at time intervals of 5 s. From Fig. 5, the non-linear pattern of the

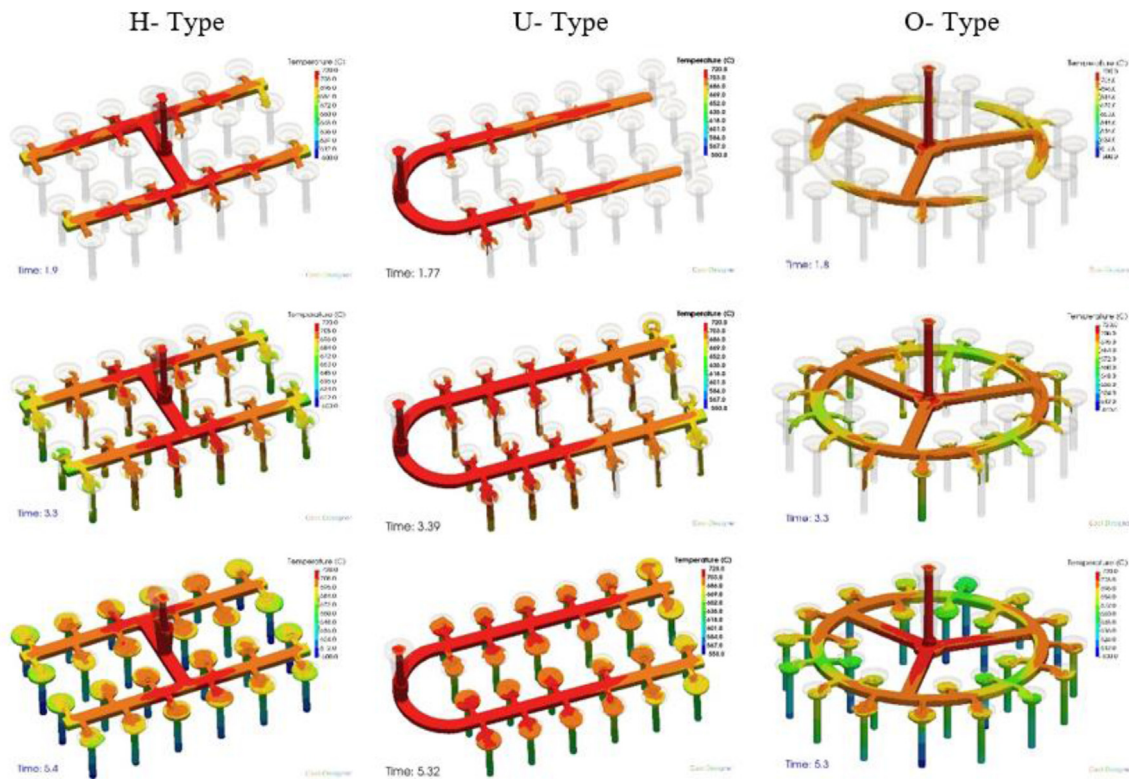


Fig. 4 – Cast design of temperature flow during simulation of three different feeding systems of FVL.

temperature curve was obtained with an increase in time in all the three forms. In comparison, thermocouple values at TC1 and TC2 demonstrated the same pattern independently based on the gating configuration, but different rates of decrease. The two thermocouples were mounted exactly at the same position at the metal-mold interface and inside the mold, away from the cavity in all the three situations. Due to heat dissipation, metal flowed from the cavity to the sand, TC2 recorded a small temperature rise that was expected. Similarly, due to the obvious large molding thickness on the outer adjacent side, TC1 displayed lower temperature value across the time spectrum. At the same time, order of the temperature plot for the thermocouples TC3, TC4 and TC5 differed in each situation. This variance can be attributed to other variables, such as thermocouple placement, cavity adjacent side thickness and complex heat source placement, among others. The

highest temperature range was observed from the thermocouples placed on the metal.

5.2.2. Experimental

In a bid to ensure the authentication of temperature data collected from the simulation study, real-time tests were also performed for the various forms of sands as well as gating configurations. Based on the experimental study, it was observed that temperature difference range was smaller with regard to various forms of sands. In spite of this, the temperature variance curve obtained from different thermocouples, using air-set sand mold, is shown in Fig. 6. Temperature data were collected using an online data acquisition device with a frequency of 5 s and a time interval of 500 s. Repeatability test of all the obtained data/measurements was performed, as an experimental approach to check the

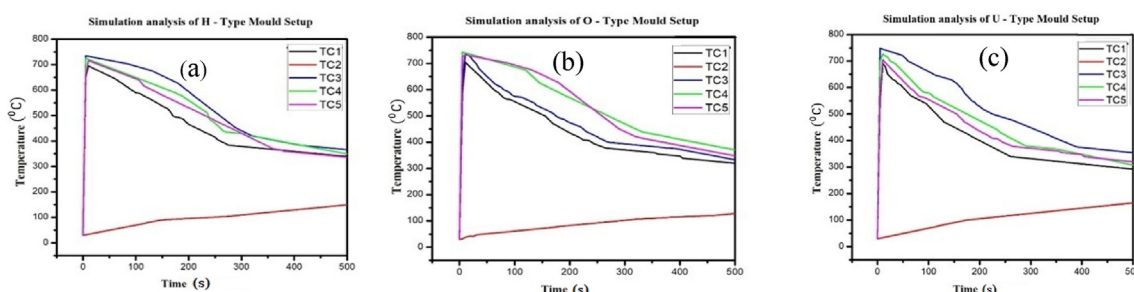


Fig. 5 – Simulation curves of the different gating designs: (a) H-, (b) O- and (c) U-type.

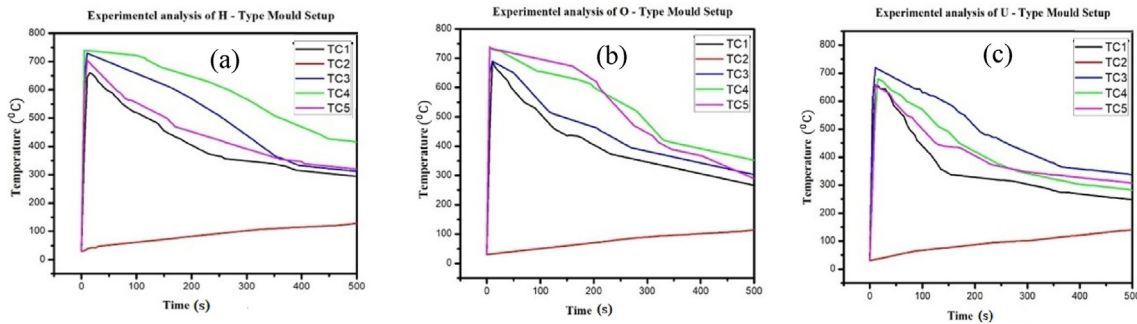


Fig. 6 – Experimental curves of different mold set-ups: (a) H-, (b) O- and (c) U-type.

reproducibility of the proposed system/FVL, the temperature data for each instance was captured three times in a similar way. Finally, in each instance, the average temperature value was obtained. Standard deviation was not calculated, because nearly the same value was obtained in all of the data points for each instance of all of the repeated tests. This verified the identical data capture and indicated the insignificance of statistical data representations.

For TC1 and TC2 thermocouples, almost identical patterns in temperature curves were obtained from the simulation results. A slight change in the order of temperature curves was observed among TC3, TC4 and TC5 thermocouple readings. This can be traced to presence of noise factors, which included humidity, air movement, sand form, heat transfer mode and interface friction. They might have influenced diffusion of the temperatures. In addition, it was observed that the range of variance obtained was limited at the end of the time span for all thermocouples in the simulation data. Whereas, the differences were shown to be large in all three types of gating designs in experimental approach. In real time, the thermocouples were placed to hit the tip of the mold and could report the precise real-time temperature of the molten metal in certain positions.

Moreover, average temperature value was then calculated to obtain difference between simulation and experimental results. Fig. 7 shows that all experimental types of gating configurations with air-set sand mold recorded lower values of average temperatures than that of simulation counterparts. In accordance with the method described in literature, the average deviation rate was determined [3]. Nearly each thermocouple displayed a variation of less than 15%, which can be used as a permissible limit according to the criterion stated in the same literature [3].

Normally, the melting temperature range of aluminium alloy lies between 550 and 615 °C. The measurement shown in TC4 thermocouple at tip of the mold, closer to the runner in H-type, showed 587 °C, which was between freezing temperature ranges. In the same direction, both TC4 and TC5 thermocouples used in O-type displayed a solidification delay. This can be assigned to an increase in the casting temperature and release of latent heat.

The experimental investigation primarily focused on the gating design, as a significant influencing factor. However, the

authors aim to find the most optimum response solutions via the appropriate use of multivariate experimental design, as a future study. This is necessary, because multivariate technique (design of experiments) is one of the best experimental designs for providing cost-effective optimum solutions, when a larger number of variables are involved in the process. It also takes into account all the relevant variables and their interactions, finding the best experimental conditions for the proper functioning of materials, devices and/or reactors. Furthermore, the relevance of application of multivariate experimental design was reported in other studies, spanning different areas, such as energy [28–31], environmental [32], sensors [33] and to mention but a few.

5.3. X-ray examination

X-ray testing was performed on chosen FVL casted components at four separate thermocouple locations: TC1, TC3, TC4 and TC5. This strategy was ideally adapted for detecting internal vulnerabilities that weaken the product strength. Many of the casting defects are volumetric in nature, and therefore it

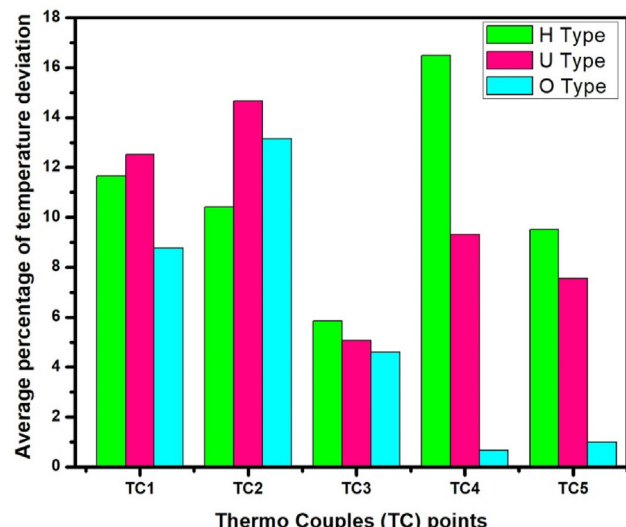


Fig. 7 – Average percentage of temperature deviation for all the types of gating designs.

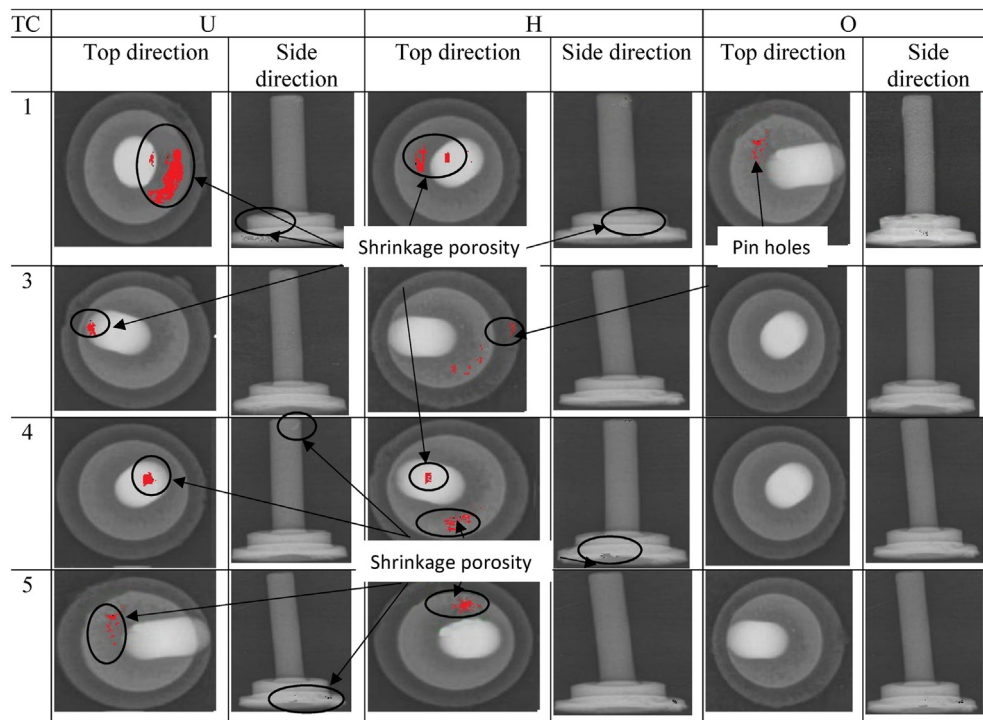


Fig. 8 – X-ray images of 24 cavities obtained from the three experimental gating designs.

is reasonably simple to identify them with this approach. These discontinuities, of course, are caused by flaws in the casting method, which, if correctly interpreted, will contribute to accurate accept-reject decisions as well as appropriate corrective action. As a result, these FVL components were machined at around 0.5 mm on all sides and subjected to X-ray examination, using a 160 peak kilo voltage device/computed radiography (CR) of Carestream unit, Coimbatore, with penetration period and current of 25 s and 5 mA, respectively. Fig. 8 shows the top and side views of X-radiographic photographs of FVL components at multiple positions of various gating designs.

Moving forward, image processing was used to predict the discontinuities with red colored label in order to precisely and clearly show the defects. As a consequence, the coding was generated in Python, using the TensorFlow Keras pre-processing image. Keras is the most advanced pre-processing method, which can read all relevant data from the uploaded file. Following that, the imported image data was translated into two arrays, utilizing the image to array feature in Numpy. The 3D image set (height, breadth and number of channels) was resized into a linear array during pre-processing level. Afterwards, the whole data collected was normalized by rescaling with the array values, dividing by 255. The frequency of each pixel value in the array data set was determined, using counter feature. According to image analysis theory, if the frequency of a pixel value is less than 60 and the pixel value is close to 0, it suggests the presence of black areas. However, in this work, the threshold value was set to 0.08, which was used to label the index of the array with any integer value. If the array index is lower than the threshold

number, it can be 111 and, if it is higher, it can be another integer, such as 222. The iteration method took place based on these integer ranges of values to calculate the index of the array and then record certain values in each of the array three channels (R, G, B). The index of the array was obtained to be 111 in the FVL casted X-ray micrographs, which produced all the pixel values in the form of R = 250, G = 0, B = 0 in three channels and marked with red color, as stated. Finally, all the data set arrays were reshaped and transformed to their original types, which can be visualized, utilizing the Matplotlib feature to track the image processing.

In all three cases of gating designs, the X-ray examination showed a few typical defects that occurred throughout the casting process. Gas porosities or blow holes were discovered on the top edge of the needles of H- and U-type of gating designs at TC1, TC3 and TC4. This can be attributed to residual gas or air contained by the metal. From H- and U-type of gating designs, the discontinuities tended to be smooth-walled rounded cavities with a spherical, elongated or flattened shape. In this analysis, an air-set sand mold was used for all the three gating designs. It might not be enough to push the gas or air out of the mold, causing the gas or air to get stuck, when the molten metal started to solidify. These porosities and blow holes, however, were not observed in O-type. It can be triggered by sudden flow of molten metal from the sprue to the cavity. Furthermore, the probability of entrapment of air or gas was understood to be dependent on the height of the sprue and the transit time of molten metal. Similarly, blow holes can be caused by the design of the sand, which was too firmly bonded, damp and has a poor permeability, due to chemical adhesion, which might have stopped gas from

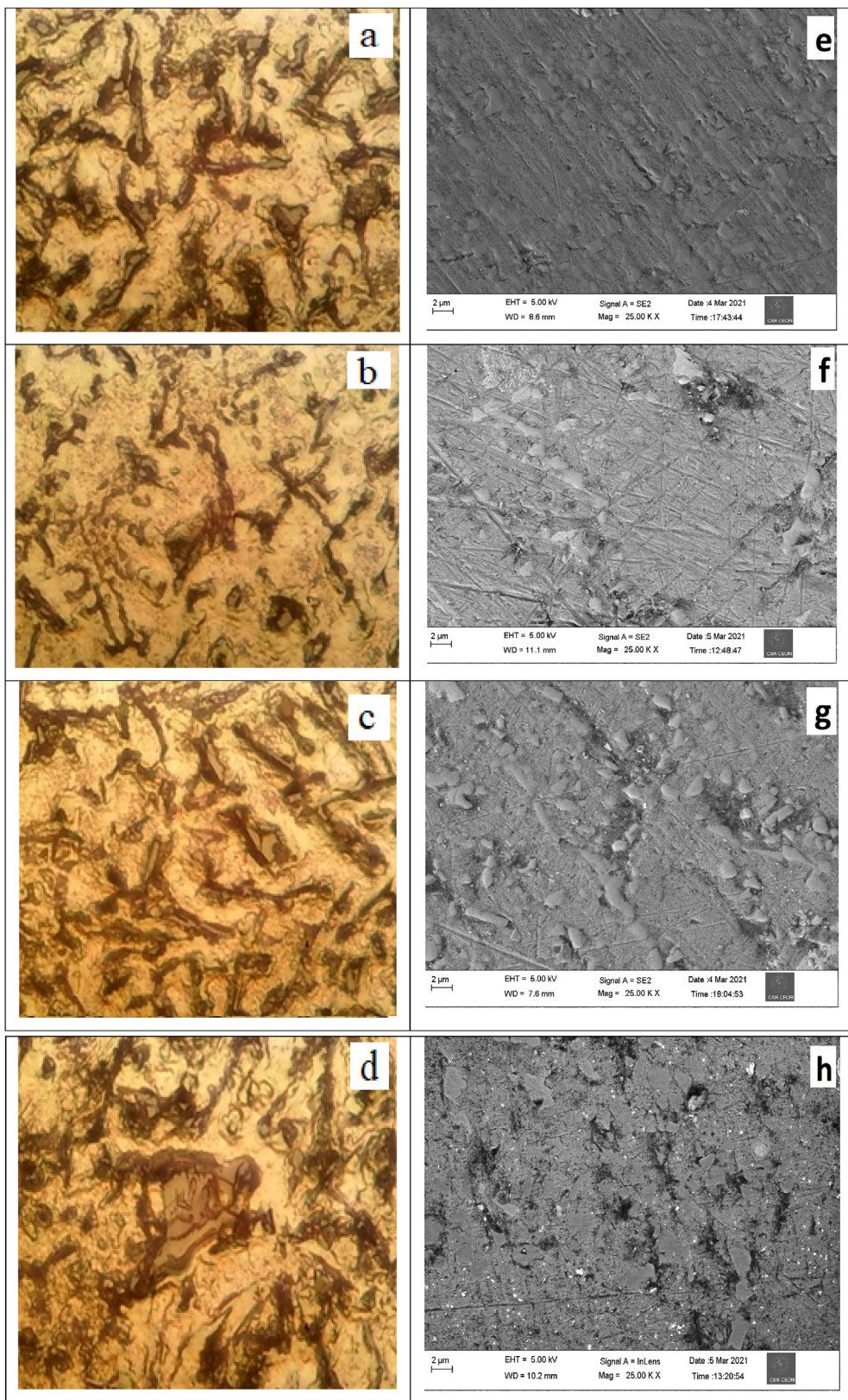


Fig. 9 – OSM images (left column), representing: (a) and (b) top face (horizontal plane), (c) and (d) cross section (vertical plane) for both TC1 and TC4 as well as SEM images (right column), showing: (e) and (f) top face (horizontal plane), (g) and (h) cross section (vertical plane) for TC1 and TC4.

escaping. Sponge shrinkage was discovered in areas of thick flank of FVL part with lacy texture and diffuse outlines, which occurred toward the mid-thickness of heavier casting pieces. Sponge shrinkage seemed to be dendritic or filamentary shrinkage, as observed with O-type of gating design from optical microscopic images obtained. These are subsequently and comprehensively discussed.

5.4. Microscopic analysis

To understand defect formation, microstructure of casted aluminium alloy was studied at specific conditions, using both optical scanning microscopy (OSM) and scanning electron microscopy (SEM). The morphological analysis was performed for O-type of gating design at two thermocouple points of TC1 and TC4. The samples were prepared in the lower part of FVL, which was designated as a sensitive part of concern by the manufacturer. Afterwards, top faces and cross-sections of the samples were perfectly polished with a 2000 grid scale. In addition, the cooling rate and air entrapment in the molten metal determined the formation of voids and pores in casting components [34]. As reported [35], unusual tortuous pores enclosed by the tips of dendrites were observed in almost all cases. However, many of the dark areas observed under optical microscope did not seem to be pores or openings, but rather to be localized irregularly formed cavities.

Figs. 9(a) and (b) show optical images of TC1 face and its cross-section, where spatial gap between the dark area was observed to be larger, whereas it was observed to be lower within the materials at cross-section. Similarly, irregular solid particles of different sizes and forms were surrounded by concentrated dendrites, as observed in Fig. 9(c), which can be attributed to discontinuous rate of cooling. There were no significant defects observed in case of outer region at TC1 sample, as shown in Fig. 9(d). This can be ascribed to the faster cooling rate at those locations, due to thick region of the mold. At same time, needle-like platelet defects (Fig. 9(e)) were apparent in the depth area, because solidification front travelled in a radial direction. It reduced rate of cooling and created a route for air bubbles through the molten metal. All of the microporosities were clearly located at inter-dendritic areas, which were consistent with reports of previous studies [36,37]. Figs. 9(f) and (g) depict the faces and depth of cross-sectional surfaces, where major defects in form of irregular pores and holes were observed. This was possible due to TC4 close vicinity runner, which disallowed molten metal to cool as quicker as TC1. The inverted positions of the casted pieces and gating configurations were specifically observed to be significant factors for evaluating microstructure and quantifying defects in the components.

5.5. Surface roughness and percentage of porosity

The value of surface roughness and percentage of porosity were measured by the results obtained from the casting products. Figs. 10 and 11 show experimental surface roughness and measured percentage of porosity values for all the three types of gating designs and sand types. The surface roughness measurement was carried out using a “cast micro finish comparator” instrument with a length of 20 mm on the

outer surface of the needle portion of FVL component. Regardless of the gating style, both air-set and sodium silicate sand molds showed a good surface finish with respect to traditional form of mold sand, as shown in Fig. 10.

Also, Fig. 10 shows that air-set sand mold casting exhibited quality surface consistency when compared with other types. This was confirmed from the lower surface roughness values obtained. The combination of additives with the pristine sand could have created strong adhesion between the sand particles and formulated the smooth surface after ramming. While the properties of the sand remained unchanged, the varied rate of solidification affected the surface roughness in all the types of gating designs. Also, the interface heat transfer coefficient and kinematic parameters of metal flow varied between the metal-mold conditions, which in turn modified the surface roughness at the outer surface. From all the designs, combination of H-type with air-set mold showed a better surface finish. Various types of molding sands might have influenced the formation of oxide layers, due to the production of gas during the reaction at metal-mold interface. Similarly, the air gap thickness was also varied, depending on the surface roughness between the metal and mold. In order to maintain dimensional consistency, the thickness of the air distance must be minimized by controlling the surface roughness value by means of a solidification method design.

To investigate the quality of finished product, percentages of porosities of all the castings were calculated using Eq. (2), as defined by Taylor et al. [38]. The experimental density was calculated, using Archimedes' principle [39].

$$\% \text{ porosity} = 100 \left(1 - \frac{\rho_L}{\rho_{th}} \times \frac{W_s}{W_s - (W_{sb} - W_b)} \right) \quad (2)$$

where;

W_s = dry weight of the casting (casting wait * number of casting).

W_{sb} = buoyant weight of casting + basket weight.

W_b = buoyant weight of basket,

ρ_L = density of liquid = 1 g/cm³ and

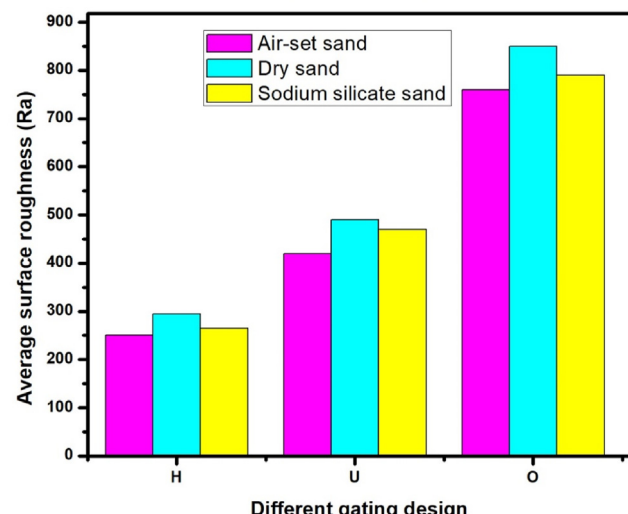


Fig. 10 – Average surface roughness of the various gating designs and sand types.

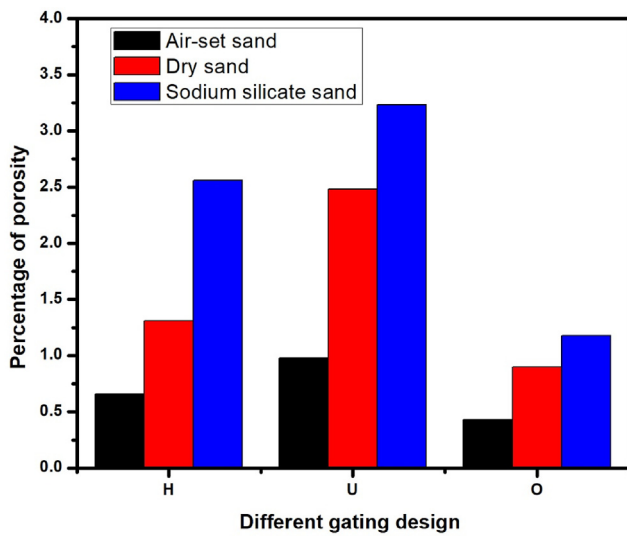


Fig. 11 – Percentage of porosity of the various gating designs and sand types.

ρ_{th} = theoretical value of porosity free density of the alloy = 2.68 g/cm³.

Keeping the form of gating configuration fixed, the percentages of porosities of all the casts were observed in the following order, air-set < dry < sodium silicate sands as seen in Fig. 11. Maintaining air-set sand mold constant, a minimum percentage of porosity was observed in O-type of gating design. From Fig. 11, it was observed that O-type of design depicted formation of air holes and production of gas was lower. It could have happened owing to the escape of air between the particles of sand and less gas formation by the lower range of freezing temperature. Also, the results of the analysis showed that a successful solidification mechanism achieved from O-type gating can be attributed to rapid cooling of the thick mold wall and feeder geometry. Porosity reduction can increase fracture toughness, which is important in impact applications [40]. Furthermore, the greater microhardness was associated with less porosity, while the uniform smooth surface of the casted samples resulted to a low surface roughness value for the chosen circumstances, as similarly reported [41]. Additionally, the relationship between characteristics, such as porosity and surface integrity with regard to microstructure and other mechanical properties [42] showed their advantages and disadvantages with respect to various factors.

6. Conclusions

FVL cast parts have been successfully manufactured and studied, using both experimental and numerical methods. Effects of H-, U- and O-type of gating designs and sand types were investigated. The study showed that the rate of cooling and solidification of metals varied significantly, depending on the configurations of the various gating systems.

The inverted position of the additively manufactured pattern minimized the risk of failure in the lower part of the component and offered a better surface finish in the mold cavity. At the same period, there was no major difference in the efficiency of the cast products with regard to sand forms. The O-style gating design allowed full mold filling at a lower pouring temperature of 750 °C. Furthermore, the kinematic parameters of molten metal and differing interlayer mold thickness were discovered to be significant factors, which influenced solidification of FVL portion in various gating designs.

Also, temperature distribution observed from numerical study matched well with the experimental analysis at the selected locations. Gas porosity, blow cracks and sponge shrinkage were discovered in the needle part and thicker portion of the flank in the FVL components for both H- and U-style of gating configurations. However, O-style of gating architecture exhibited irregular form of cracks and needle-like solid particles were observed only at TC4 site. They were very near to the sprue discharge port. Only smooth surface morphology was present at TC1 of O-style layout. This can be attributed to fast mold filling, which could have minimized the chances of air trapping, porosity and shrinkage.

Finally, the decreasing order of percentage of porosity was obtained in the following order of types of sands used: air-set < dry < sodium silicate. Based on overall efficiency, the O-type of gating design was identified as the most suitable design for large-scale quality production of FVL in pump industries.

Declaration of Competing Interest

The authors declare that they have no known competing financial interests or personal relationships that could have appeared to influence the work reported in this paper.

Acknowledgement

The authors thank Kalasalingam Academy of Research and Education, Krishnankoil for providing the facilities for various tests and characterizations. The King Saud University authors extend their appreciation to the Deanship of Scientific Research at King Saud University for funding the work through the research group project no. RG-148. This Research was funded by King Mongkut's University of Technology North Bangkok has received funding support from the National Science, Research and Innovation Fund (NSRF) (Grant No. KMUTNB-MHESI-64-16.1).

REFERENCES

- [1] Mia M, Sharma S, Singh J, Gupta MK, Dwivedi SP, Saxena A, et al. Investigation on mechanical, tribological and microstructural properties of Al–Mg–Si–T6/SiC/muscovite-hybrid metal-matrix composites for high strength applications. *J Mater Res Technol* 2021;12:1564–81.

- [2] Contatori C, Domingues Jr NI, Barreto RL, de Lima NB, Vatavuk J, Borges AAC, et al. Effect of Mg and Cu on microstructure, hardness and wear on functionally graded Al–19Si alloy prepared by centrifugal casting. *J Mater Res Technol* 2020;9(6):15862–73.
- [3] Karthik A, Srinivasan SA, Karunanithi R, Babu SK, Jain VKS. Influence of CeO₂ reinforcement on microstructure, mechanical and wear behavior of AA2219 squeeze cast composites. *J Mater Res Technol* 2021;14:797–807.
- [4] Mohiuddin MV, Hussainy SF, Krishnaiah A, Laxminarayana P. Experimental investigation to produce thin-walled sand-casting using combination of casting simulation and additive manufacturing techniques. *Int J Adv Manuf* 2017;90(9):3147–57.
- [5] Kermanpur A, Mahmoudi S, Hajipour A. Numerical simulation of metal flow and solidification in the multi-cavity casting moulds of automotive components. *J Mater Process Technol* 2008;206(1–3):62–8.
- [6] Yajjala RK, Inampudi NM, Jinugu BR. Correlation between SDAS and mechanical properties of Al–Si alloy made in Sand and Slag moulds. *J Mater Res Technol* 2020;9(3):6257–67.
- [7] Shishegaran A, Saeedi M, Mirvalad S, Korayem AH. The mechanical strength of the artificial stones, containing the travertine wastes and sand. *J Mater Res Technol* 2021;11:1688–709.
- [8] Eco-friendly concrete containing recycled plastic as partial replacement for sand. *J Mater Res Technol* 2020;9(4):4631–43.
- [9] Ravi B, Pal DK. Rapid casting development. In rapid manufacturing seminar. Teamtech; 2006.
- [10] Nimbalkar SL, Dalu RS. Design optimization of gating and feeding system through simulation technique for sand casting of wear plate. *Perspect Sci* 2016;8:39–42.
- [11] Vijayaram TR, Sulaiman S, Hamouda AMS, Ahmad MHM. Numerical simulation of casting solidification in permanent metallic molds. *J Mater Process Technol* 2006;178(1–3):29–33.
- [12] Jafari H, Idris MH, Shayganpour A. Evaluation of significant manufacturing parameters in lost foam casting of thin-wall Al–Si–Cu alloy using full factorial design of experiment. *T Nonferr Metal Soc* 2013;23(10):2843–51.
- [13] Pedersen KM, Tiedje N. Temperature measurement during solidification of thin wall ductile cast iron. Part 1: theory and experiment. *Measurement* 2008;41(5):551–60.
- [14] Choudhari CM, Narkhede BE, Mahajan SK. Casting design and simulation of cover plate using AutoCAST-X software for defect minimization with experimental validation. *Procedia Manuf* 2014;6:786–97.
- [15] SH MR, Raikar PU. Yield improvement of cast Part Using computer aided casting simulation. *Int Res J Eng Technol* 2015;2:858–62.
- [16] Ravi B. Metal casting: computer-aided design and analysis. PHI Learning Pvt. Ltd.; 2005.
- [17] Rajkumar I, Rajini N, Alavudeen A, Prabhu TR, Ismail SO, Mohammad F, et al. Experimental and simulation analysis on multi-gate variants in sand casting process. *J Manuf Process* 2021;62:119–31.
- [18] Rao PP, Chakravarthi G, Kumar ACS, Balakrishna B. Application of casting simulation for sand casting of a crusher plate. *Int J Therm Technol* 2011;1(1):107.
- [19] Rajkumar I, Rajini N. Metal casting modeling software for small scale enterprises to improve efficacy and accuracy. *Mater Today* 2021;46(17):7866–70.
- [20] Khade US, Nimbalkar V. Application of 3D CAD modeling and casting simulation to eliminate casting defects. *Int J Res Advent Technol* 2016;1–5.
- [21] Rajkumar I, Rajini N. Influence of parameters on the smart productivity of modern metal casting process: an overview. *Mater Today* 2021. In press.
- [22] Mandaliya PJ, Dave JT. Study of piston sleeve manufactured by sand casting process to reduce rejection rate using simulation software. *Int J Mech Prod Eng Res Dev* 2013;3(2):161–8.
- [23] Masoumi M, Hu H, Hedjazi J, Bouterabi M. Effect of gating design on mold filling. *Trans Amer Foundry Soc* 2005;113:185–96.
- [24] Francis V, Jain PK. Experimental investigations on fused deposition modelling of polymer-layered silicate nanocomposite. *J Virt Phys Prot* 2016;11(2):109–21.
- [25] Lee CW, Chua CK, Cheah CM, Tan LH, Feng C. Rapid investment casting: direct and indirect approaches via fused deposition modelling. *Int J Adv Manuf Technol* 2004;23(1):93–101.
- [26] Mohiuddin MV, Hussainy SF, Krishnaiah A, Laxminarayana P, Sundarrajan S. Experimental study of sand mold process parameters on Al-alloy sand castings using DoE. *IOSR J Mech Civ Eng* 2014;11(6):1–6.
- [27] Mohiuddin MV, Krishnaiah A, Hussainy SF. Influence of sand molding process parameters on product quality of Al-Si alloy casting - an ANOVA approach. *Int J Adv Res Sci Eng* 2015;4(1):1751–60.
- [28] Galliano S, Bella F, Bonomo M, Viscardi G, Gerbaldi C, Boschloo G, et al. Hydrogel electrolytes based on xanthan gum: green route towards stable dye-sensitized solar cells. *Nanomaterials* 2020;10(8):1585.
- [29] Bella F, Pugliese D, Nair JR, Sacco A, Bianco S, Gerbaldi C, et al. A UV-crosslinked polymer electrolyte membrane for quasi-solid dye-sensitized solar cells with excellent efficiency and durability. *Phys Chem Chem Phys* 2013;15(11):3706–11.
- [30] Bella F, Imperiya M, Ahmad A. Photochemically produced quasi-linear copolymers for stable and efficient electrolytes in dye-sensitized solar cells. *J Photochem Photobiol A* 2014;289:73–80.
- [31] Galliano S, Bella F, Bonomo M, Giordano F, Gratzel M, Viscardi G, et al. Xanthan-based hydrogel for stable and efficient quasi-solid truly aqueous dye-sensitized solar cell with cobalt mediator. *Sol RRL* 2021;5:2000823.
- [32] Elik A, Bingol D, Altunay N. Ionic hydrophobic deep eutectic solvents in developing air-assisted liquid-phase microextraction based on experimental design: application to flame atomic absorption spectrometry determination of cobalt in liquid and solid samples. *Food Chem* 2021;350:129237.
- [33] Hsieh CZ, Chung WH, Ding WH. Experimental design approaches to optimize ultrasound-assisted simultaneous silylation dispersive liquid–liquid microextraction for the rapid determination of parabens in water samples. *RSC Adv* 2021;11(38):23607–15.
- [34] Yousefian P, Tiryakioglu M. Pore formation during solidification of aluminum: reconciliation of experimental observations, modeling assumptions, and classical nucleation theory. *Mater Trans* 2018;49(2):563–75.
- [35] Li Z, Jing Y, Guo H, Sun X, Yu K, Yu A, et al. Study of 3D pores and its relationship with crack initiation factors of aluminum alloy die castings. *Mater Trans B* 2019;50(3):1204–12.
- [36] Plancher E, Gravier P, Chauvet E, Blandin JJ, Boller E, Martin G, et al. Tracking pores during solidification of a Ni-based superalloy using 4D synchrotron micromotography. *Acta Mater* 2019;181:1–9.
- [37] Pham MS, Dovgyi B, Hooper PA, Gourlay CM, Piglione A. The role of side-branching in microstructure development in laser powder-bed fusion. *Nat Com* 2020;11(1):1–12.
- [38] Taylor RP, McClain ST, Berry JT. Uncertainty analysis of metal-casting porosity measurements using Archimedes principle. *Int J Cast Met Res* 1999;11(4):247–57.

- [39] Lus HM. Effect of casting parameters on the microstructure and mechanical properties of squeeze cast A380 aluminum die cast alloy. *Kovove Mater* 2012;50(4):243–50.
- [40] Di Giovanni MT, de Menezes JT, Cerri E, Castrodeza EM. Influence of microstructure and porosity on the fracture toughness of Al-Si-Mg alloy. *J Mater Res Technol* 2020;9(2):1286–95.
- [41] Sheshadri R, Nagaraj M, Lakshmikanthan A, Chandrashekappa MPG, Pimenov DY, Giasin K, et al. Experimental investigation of selective laser melting parameters for higher surface quality and microhardness properties: taguchi and super ranking concept approaches. *J Mater Res Technol* 2021;14:2586–600.
- [42] Gupta MK, Singla AK, Ji H, Song Q, Liu Z, Cai W, et al. Impact of layer rotation on micro-structure, grain size, surface integrity and mechanical behavior of SLM Al-Si-10Mg alloy. *J Mater Res Technol* 2020;9(5):9506–22.